Spray-Dried Multiscale Nano-biocomposites Containing Living Cells

Patrick E. Johnson,[†,⊥] Pavan Muttil,[‡] Debra MacKenzie,[‡] Eric C. Carnes,[#] Jennifer Pelowitz,[#] Nathan A. Mara,[∥,∞] William M. Mook,[∥] Stephen D. Jett,[§] Darren R. Dunphy,[⊥] Graham S. Timmins,[*,‡] and C. Jeffrey Brinker[*,⊥,#]

[†]Departments of Nanoscience and Microsystems Engineering, [‡]Pharmaceutical Sciences, [§]Cell Biology and Physiology, and [⊥]Chemical and Biological Engineering, Center for Micro-Engineered Materials, University of New Mexico, Albuquerque, New Mexico 87106, United States, [∥]Center for Integrated Nanotechnologies, [∞]Institute for Materials Science, Los Alamos National Laboratories, Los Alamos, New Mexico 87545, United States, and [#]Advanced Materials Laboratory, Sandia National Laboratories, Albuquerque, New Mexico 87185, United States

ABSTRACT Three-dimensional encapsulation of cells within nanostructured silica gels or matrices enables applications as diverse as biosensors, microbial fuel cells, artificial organs, and vaccines; it also allows the study of individual cell behaviors. Recent progress has improved the performance and flexibility of cellular encapsulation, yet there remains a need for robust scalable processes. Here, we report a spray-drying process enabling the large-scale production of functional nano-biocomposites (NBCs) containing living cells within ordered 3D lipid–silica nanostructures. The spray-drying process is demonstrated to work with multiple cell types and results in dry powders exhibiting a unique combination of properties including highly ordered 3D nanostructure, extended lipid fluidity, tunable macromorphologies and aerodynamic diameters, and unexpectedly high physical strength. Nanoindentation of the encasing nanostructure revealed a Young's modulus and hardness of 13 and 1.4 GPa, respectively. We hypothesized this high strength would prevent cell growth and force bacteria into viable but not culturable (VBNC) states. In concordance with the VBNC state, cellular ATP levels remained elevated even over eight months. However, their ability to undergo resuscitation and enter growth phase greatly decreased with time in the VBNC state. A quantitative method of determining resuscitation frequencies was developed and showed that, after 36 weeks in a NBC-induced VBNC, less than 1 in 10 000 cells underwent resuscitation. The NBC platform production of large quantities of VBNC cells is of interest for research in bacterial persistence and screening of drugs targeting such cells. NBCs may also enable long-term preservation of living cells for applications in cell-based sensing and the packaging and delivery of live-cell vaccines.

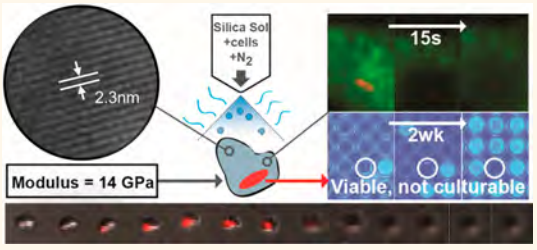

KEYWORDS: viable-but-not-culturable cells · biopreservation · bacterial persistence · cellular · encapsulation · sol–gel · spray drying · evaporation-induced self-assembly

Due to the unique behaviors and characteristics of encapsulated cells and their applications to biosensing, catalysis, and biomedical research, cell-based bioinorganic materials have been the subject of intense study since the first demonstration of physical entrapment of cells within silica gels by Carturan *et al*. over 20 years ago.[1] Since then, efforts to incorporate living cells in inorganic gels and nanostructures have burgeoned to include encapsulation within glycerol-based silica gels,[2,3] calcium mineral layers,[4] vapor phase sol–gel matrices,[5,6] and solution phase lipid–silica matrices.[7] These studies have sought to enhance cell viability by reducing cellular stress resulting from chemical byproducts of the encapsulation process,[7] increasing cell resistance to processing stresses and lytic enzymes,[4] and improving chemical and mechanical stability,[2] while enabling extension of the respective encapsulation methods to a wider range of cell types.[6] Significant improvements in biofunctionality have been achieved, but each of the methods has limitations that reduce its general applicability including limited long-term viability,[2] thin-film architectures with correspondingly low material yields,[7] and limited success in cell lines other than *Escherichia coli* (*E. coli*) and yeast, which are thought to survive harsh processing conditions due to their robust cell walls.

In order to preserve cell functionality and accessibility in a nominally dry, "solid-state" miniaturized sensor without the need of an

* Address correspondence to gtimmins@salud.unm.edu, cjbrink@sandia.gov.

Received for review February 18, 2015 and accepted June 4, 2015.

Published online 10.1021/acsnano.5b01139

© XXXX American Chemical Society

external fluidic system, Baca *et al*. developed a process referred to as cell-directed assembly (CDA).[7] In CDA, amphiphilic short-chain lipids serve as structure-directing agents to organize hydrophilic silicic acid precursors into highly ordered periodic lipid–silica mesophases *via* evaporative processes such as spin-coating. If bacteria, yeast, or other cells in liquid suspension are added to the precursor solution, evaporation results in a highly conformal and coherent 3D lipid–silica nanostructure that surrounds the cell. This technique inherently has the advantage of low-temperature processing conditions and relatively brief cell–solvent contact times, which, in themselves, can result in increased cell stress and death.[5] Using a live/dead assay on encapsulated *Saccharomyces cerevisiae*, Baca *et al*. reported viabilities exceeding 50% after 4 weeks of storage at room temperature (RT).[7] The CDA process was extended to an aerosol spraying process that allowed individual *Staphylococcus aureus* (*S. aureus*) bacteria to be physically and chemically isolated within 3D nanostructured droplets deposited on glass.[8] Nanoconfinement of individual *S. aureus* was shown to result in cellular self-sensing of exported signaling molecules, triggering the induction of quorum sensing pathways and consequent genetic reprogramming of the cell to its pathogenic phenotype with associated increases in long-term viability.[8] This suggests that, beyond preserving cellular viability under harsh conditions, 3D encapsulation of isolated cells may also direct desired or unanticipated changes in cellular behavior due to confinement induced chemical or mechanical cues.

Although simple in its preparation, the absolute yield of CDA is very limited, and we hypothesized that, using scalable spray drying, CDA could be adapted to the large-scale production of cell-encapsulating composites with retained biofunctionality. Industrial spray driers are routinely used in the pharmaceutical and food industries due to their ease of use, diverse range of liquid precursors, and high product yield and consistency. Furthermore, spray drying can easily be scaled from prototype benchtop instruments to large, industrial-scale units. The process of spray drying involves injecting a solution of liquid precursors *via* a heated nozzle into a stream of a carrier gas. The liquid is aerosolized into droplets that have a well-controlled average size and a broad but reproducible size distribution. The droplets proceed through an array of glass cylinders designed to allow adequate residence times for solvent evaporation to yield individual, dry particles. The particles then exit the flow of the gas and collect into a vessel, while the carrier gas is exhausted through a vacuum aspirator. Spray drying is attractive in part due to the wide range of precursors that can be used including pharmaceuticals,[9] sugars,[10–12] lipids and fats,[13,14] milk sugars and proteins,[15] drugs and antibiotics,[13] polymers,[16] and other biomolecules.[17,18] More recently, reports of spray-dried cell suspensions indicate that this technique is applicable to attenuated virus vaccines[19] and live bacterial vaccines.[12,20]

Here, we describe the first demonstration of spray-dried NBC materials in which living cells are encapsulated within a protective lipid–silica nanostructured matrix by evaporation-induced CDA. The spray-dried NBC materials are shown to be mechanically robust, with controlled structures spanning the nanoscale to microscale regimes depending on spray-drying conditions. The biofunctionality of NBC-encapsulated *E. coli* is preserved for months, as shown using a probe for intracellular ATP (exogenous ATP is known to degrade rapidly, providing a null signal after <96 h at 4 °C)[21] and growth culturing assays. On the basis of ease of processing and the ability to engineer both the nano-biointerface and macroscopic aggregate morphology/aerodynamic diameter, we feel that the NBC spray-drying process should have broad applicability in pharmacology, cell-based sensing, microbial fuel cells, vaccines, and fundamental studies of biology at the individual and multiple cell scales.

RESULTS AND DISCUSSION

Spray Drying of Lipid–Silica Nano-biocomposites. Evaporation-induced self-assembly (EISA) of highly ordered lipid–silica matrices encapsulating cells referred to as CDA[7,8] is an established technique for the preparation of living biomaterials. Here, we expanded the breadth of this process by adapting it to spray drying using a commercial benchtop spray drier fitted with a custom collection receptacle (see Figure 1 for a schematic of the experimental setup). The spray-dry process involves the delivery of liquid precursors to a heated nozzle, which injects the solution into a nitrogen gas sheath that is maintained by vacuum aspiration through the top of the cyclone. The solution dries within the heated sheath gas, and the dried powder collects into a vial. By systematic modulation of primary control parameters such as the ratio of the nitrogen gas flow rate to the liquid feed rate, the average liquid droplet size can be varied over the approximate range from less than 10 μm to over 100 μm, resulting in dried particles with rather broad particle size distributions ranging from ~0.5 to 25 μm. Depending on the Peclet number (*vide infra*), morphologies can be varied from compact irregular particles to hollow, more spherical shapes.

Lipid–silica precursor solutions (termed precursor sols) were prepared according to the method of Baca *et al*.[7] as summarized in the Materials and Methods section and Supplemental Figure 1. Our initial studies employed *E. coli* bacteria expressing a red fluorescent protein (RFP) variant (pDsRed-Express 2, Clontech, Mountain View, CA, USA) in liquid culture or green fluorescent latex beads of comparable size and surface charge as *E. coli*[22] as a control. The initial spray-drying parameters (nozzle temperature, solution feed rate,

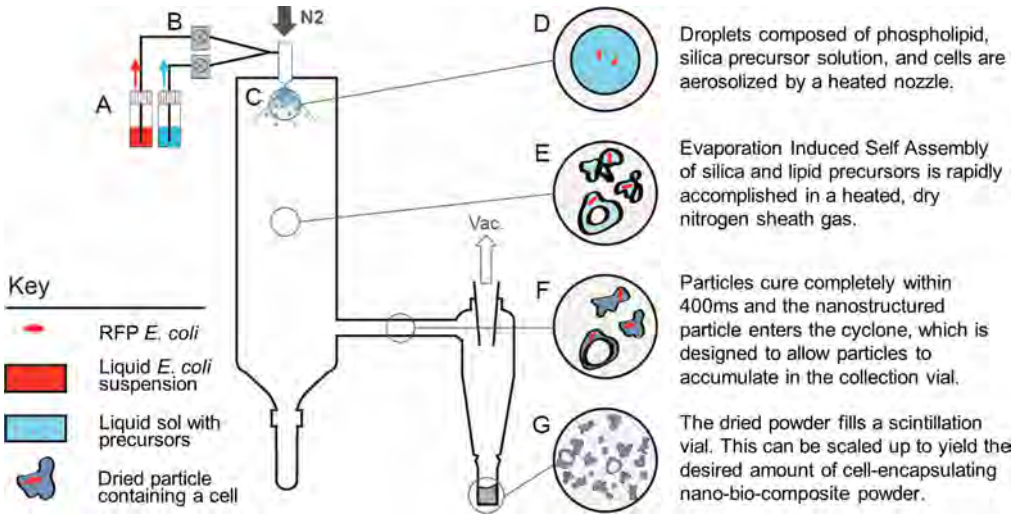

Figure 1. Schematic of the spray-drying process using a Büchi B-290 mini spray drier for the production of lipid−silica NBCs. Solutions of cells in liquid suspension and lipid−silica precursors are mixed in scintillation vials (A) and dispensed into the sprayer nozzle *via* peristaltic pumps with mixing immediately prior to injection with a Y valve (B). This mixture is aerosolized by the heated nozzle in a sheath of N_2 gas (C). Droplets are ∼10−100 μm in diameter and consist of cells, lipid (an inhomogeneous mixture of free, micellular, or liposomal lipids), silica precursors, and solvent (D). The droplet size can be varied by changing the ratio of the N_2 gas flow rate to that of the liquid feed rate. (E) Lipids organize silica precursors into an ordered nanostructure as the solvent evaporates during EISA. (G) Particles are fully dried before entering the cyclone (F) and flow through the cyclone vortex into the collection chamber. An aspiration vacuum pump (Vac.) pulls a vacuum on the assembly, exhausting N_2.

TABLE 1. Process Parameters Tested within This Study Define the Limits of Powder Formation[a]

user-defined process parameters	range tested	notes
nozzle temperature	60−120 °C	<60 °C: no powder formation >120 °C: not tested
solution feed rate	2.5−4.5 mL/min	<2.5 mL/min: not tested >4.5 mL/min: no powder formation
sheath gas flow rate	30−60 L/h	<30 L/h: no particle formation 60 l/h: maximum flow rate
vacuum aspiration level	90−100%	<90%: no particle collection 100%: maximum level

[a] The outlet temperature for all processes tested remained between 30 and 45 °C depending on the inlet temperature and the solution feed rate.

gas flow rate, and vacuum aspiration level; see Table 1) were chosen based on previous studies of spray drying of cells incorporated within sucrose−trehalose matrices.[19] *E. coli* cells in phosphate-buffered saline (PBS) and the precursor sol were dispensed into separate scintillation vials and delivered to the heated nozzle with two peristaltic pumps, one for each solution (Figure 1A). Up to this point, cells remained in PBS suspension for <30 min and were ∼96% viable, as confirmed with live/dead viability staining (Supplemental Figure 9). The solutions were combined immediately prior to injection into the drier nozzle (Figure 1B). This method minimizes cell contact time with precursor sol constituents (∼15% ethanol v/v and pH 3), allowing for increased cell viability.[23] Aerosolization of the solution (Figure 1C) occurs in a sheath of heated nitrogen gas (inlet temperatures ranged from 60 to 120 °C), where the aerosolized liquid droplets (Figure 1D) were estimated to range from 50 to 100 μm in diameter[16] depending on the processing parameters. Solvent evaporation from the droplets within the heated nitrogen stream progressively increases the concentration of nonvolatile precursor sol constituents and drives self-assembly of the droplets into periodic, ordered lipid−silica mesophases (*vide infra*) in a manner related to aerosol-assisted EISA (Figure 1E) reported previously[24] and reviewed recently by Boissiere *et al.*[25] Ensuing evaporation and thermally driven condensation of the soluble silica precursors solidifies the particles (Figure 1F) as they enter the cyclone, exit the gas flow, and collect within the sample chamber (Figure 1G). After completion of a drying cycle, the collection vial is removed from the cyclone and the powder is dispensed into individual containers for storage. The residence time of the aerosolized droplet within the spray dryer was estimated to be ∼400 ms based on a literature report for a similar spray-drying setup[12] and is considerably shorter than that of aerosol-assisted EISA (∼3−6 s) performed at a lower Reynolds number[24,25] or CDA, which requires ∼1 min to achieve complete drying following spin-coating.[7] The outlet temperature measured just before the point that particles enter the cyclone remained below 45 °C for all spray-drying parameters used in this study. We hypothesize that the combined low outlet temperature and short residence time serve to reduce heat transfer to the encapsulated cells,[26] improving conditions for maintaining high cell viability.

TABLE 2. Macrostructural and Nanostructural Characteristics of Spray-Dried NBC Particles As a Function of Spraying Parameters Referred to as Processes A–E

process	parameters: nozzle temp (°C), feed rate (mL/min)	hollow particle fraction (%)[a]	particle diameter (μm)	fine particle MMAD (μm)[b]	geometric standard deviation (μm)	nanostructure peak (°2θ)
A	60 °C, 3.5 mL/min	[c]	13.2 ± 1.7	6.74	1.15	2.88 ± 0.04
B	90 °C, 3.5 mL/min	19.4	16.7 ± 4.8	3.29	1.88	2.92 ± 0.01
C	120 °C, 3.5 mL/min	26.4	20.8 ± 2.7	3.99	2.99	2.85 ± 0.06
D	90 °C, 2.5 mL/min	31.7	21.3 ± 2.6	2.66	1.78	2.90 ± 0.02
E	90 °C, 4.5 mL/min	[c]	16.8 ± 2.5	3.70	2.64	2.87 ± 0.03

[a] The hollow particle fraction is the observed percentage contribution of hollow particles within a spray-dried sample. [b] The fine particle fraction is the fraction of powder from which large aggregates of particles have been removed. MMAD: mass mean aerodynamic diameter. [c] The sample contained no distinguishable hollow particles.

Particle Macrostructure and Size Characteristics but Not Nanostructure Are Dependent on Spray Parameters. Under all conditions investigated, we found that either latex beads or bacteria were necessary for particle formation and capture; their absence led to no particle accumulation in the collection vial but instead resulted in a thick, dense film on the inside of the cyclone and sample collection chamber. This behavior suggests that, for the rather dilute precursor sol used here, the formation of large particles (>1 μm) that can be concentrated and collected in the cyclone requires an effective nucleation site upon which to condense the lipid–silica encapsulating matrix. With or without cells or beads, smaller, spherical nanostructured lipid–silica particles (<1 μm) likely form as described for aerosol-assisted EISA,[24,25,27,28] but these are drawn by vacuum into the spray-drier aspiration filter and are not collected by the Büchi B-290 cyclone. To support this hypothesis, we performed aerosol-assisted EISA using the identical precursor sol as for spray drying and a TSI aerosol generator and formed ordered, spherical, lipid–silica mesophase particles with sizes ranging from 20 nm to 1 μm (see Supplemental Figure 2 and associated text for images and experimental details).

For the cell- or bead-containing samples, we observed a strong dependence of particle formation and morphology on spray-drying parameters. To establish processing structure–property relationships, we systematically varied the four independent processing control parameters of our spray-drying system—nozzle temperature, solution feed rate, sheath gas flow rate, and vacuum aspiration level (Table 1)—and analyzed the effect on macromorphology, hydrodynamic size, aerodynamic size, and nanostructure (Table 2). Nozzle temperature and solution feed rate were identified to be the most critical parameters. Nozzle temperatures below 60 °C and feed rates above 4.5 mL/min resulted in no collectible particles. For these spray drying parameters (low inlet temperature and high feed rate), insufficient heat transfer occurs to the sprayed droplets and partially dried droplets adhere readily to the walls of the spray chamber/cyclone.[29,30] This tendency is known to occur in particular for droplets containing lipids, where coalescence and adherence to the spray chamber is reported to occur if the product does not dry immediately (milliseconds) after spraying.[31] Temperatures exceeding 120 °C were not investigated due to potential heat stresses on the cells, and we did not test lower feed rates due to apparatus limitations. Other process parameters such as sheath gas flow rate and vacuum aspiration level were shown to impact only particle yield and were not studied further. The process parameters and their qualitative effects on particle formation are summarized in Table 1.

With respect to particle macromorphology, using fluorescence optical microscopy and scanning electron microscopy (SEM), we observed three distinct classes of particles that were dependent on the spraying parameters: large, solid aggregates (Figure 2A–C); smaller, "raisin-like" solid particles (Figure 2D–F); and spherical, hollow particles with varying sizes (Figure 2G–I). These macroscopic features (summarized in Table 2) are generally consistent with those of other spray-dried materials reported in the literature.[32] Samples that were prepared at low temperature and/or high feed rate (*i.e.*, process A) typically consisted of large solid particles that are observed to be aggregates of smaller particles. This clumping behavior is explained by the relatively high moisture content and the large lipid fraction of the NBCs.[33] Samples that were prepared at high temperature and/or low feed rate (*i.e.*, process D) consisted of smaller discrete particles with a subpopulation that were hollow and spherical with a distinct outer shell or crust as described by M. Farid.[34] However, regardless of macrostructure, both low-angle X-ray diffraction (XRD) (Table 2) and transmission electron microscopy (TEM) (Figure 4) revealed a very highly ordered periodic nanostructure that was independent of spray-drying conditions. The XRD peak at $2\theta \approx 2.9°$ is consistent with a hexagonal or lamellar lipid–silica mesophase (*vide infra*) with a characteristic *d*-spacing of ~2.3 nm, similar to that formed *via* EISA of thin films or droplets[7,8,35,36] (see Supplemental Figure 7 for XRD analysis of control thin films and aerosol-assisted EISA particles).

As has been established by theoretical and experimental investigations of particle formation during

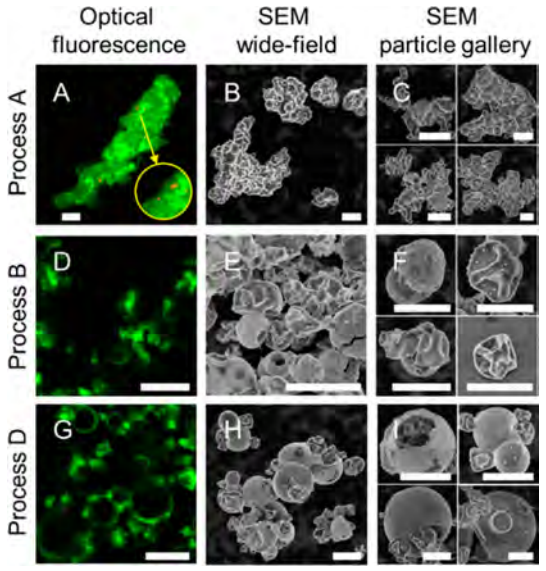

Figure 2. Particle macromorphology can be tuned depending on the spray-drying parameters listed in Table 1 to yield large or small particles with varying percentages of hollow particles. (A−C) Large particles and/or aggregates prepared with process A can contain multiple red-fluorescent bacteria (K12 *E. coli* constitutively expressing pDsRed-Express 2, an RFP variant) (A, inset), and particle aggregates can range from ~10 to 30 μm or larger (B, C). (D−F) Individual particles prepared with higher temperatures in process B demonstrate smaller particles, which are more disperse, are less prone to aggregation, and contain a subpopulation of hollow particles. (G−I) Lower feed rates reveal a higher fraction of hollow particles with a mixed size distribution; an optical slice of <0.5 μm allows for the cross-sectional visualization of hollow particles (G). Samples were prepared using a green fluorescent lipid, which extends throughout the particle. The scale bar is 5 μm.

conventional spray drying,[37,38] a major determinant of particle macromorphology is the Peclet number (Pe), defined as the (rate of evaporation)/(rate of diffusion) where the evaporation rate and diffusion rate are complex and depend in turn on parameters such as temperature, droplet size, concentration, residence time, and carrier gas relative pressures in volatile species.[25,39] At low Pe (<1) the solutes can diffuse toward the particle center to accommodate the reduced volume resulting from evaporation. This results in smaller, denser particles. At Pe > 1 the solute molecules have insufficient time to distribute within the droplet. This results in solute enrichment on the droplet surface. The higher the evaporation rate, the sooner the surface reaches "supersaturation", causing solidification. Further drying creates hollow particles whose size increases and density decreases with increasing Pe.[38] These particles may or may not wrinkle or buckle upon complete drying due to thermal or capillary "drying" stresses. In our experiments, we determined the percentage fraction of hollow particles within a sample by counting >300 particles per sample from different SEM images and differentiating between solid (dense and ill-defined shapes) and hollow (swollen and spherical) particles. We found larger fractions of hollow particles with increasing inlet (nozzle) temperatures and decreasing solution feed rates (data summarized in Table 2). Both these conditions increase heat transfer to the droplet surface, increasing Pe and causing solidification of the droplet exterior to occur at an earlier stage of drying when the particle volume is still large.[34] Further solvent removal by diffusion produces hollow particles.[40] Spray drying with a lower inlet temperature (*e.g.*, 60 °C) and/or higher feed rate (*e.g.*, 4.5 mL/min) did not result in hollow particles and, in general, yielded larger, solid aggregates. On the basis of XRD and TEM analysis (*vide infra*), after solidification of the particle surface, we determined that the remainder of the precursor solution or liquid crystalline mesophase can continue to self-assemble into an ordered nanostructure on the interior shell wall, within a separate particle enclosed by the hollow particle, or within a solid particle (*e.g.*, Figure 2). Here, it should be pointed out that, compared to aerosol-assisted evaporation induced self-assembly,[24,25,27,28] the conventional spray-drying process we employed is characterized by a higher Pe (higher inlet temperature and carrier gas feed rate), increasing the likelihood of forming hollow particles, as previously demonstrated by Bruinsma *et al.*, who formed hollow mesoporous silica particles *via* EISA using a Büchi B-190 mini spray dryer operating at an outlet temperature of 76 °C.[41] In comparison, for aerosol-assisted EISA, hollow particles have been reported only under limited conditions, for example at high temperature using high-volatility solvents (high Pe)[26] or *via* addition of $(NH_4)SO_4$, which phase separates and thermally decomposes, serving as a "bloating" agent.[42] Consistent with these arguments, Supplemental Figure 2 shows solid, spherical lipid/silica mesophase particles formed *via* aerosol-assisted EISA using the identical precursor sol to that for spray drying (see Supplemental Figure 2 for experimental details).

To quantify particle size, we analyzed powders from each of the processes for particle hydrodynamic size using laser diffractometery (Supplemental Figure 3A). The particle size distribution and the geometric standard deviation were found to fall between 13 and 21 μm and 1−3 μm, respectively, for all of the processes tested (data summarized in Table 2). The aerodynamic properties of dried powders were analyzed by determining the mass mean aerodynamic diameter (MMAD), which is used to simulate dry powder inhalation into and deposition within the lung.[43] This was performed by dry injecting the powders with an insufflator into a steady flow of nitrogen gas flowing through a multistage cascade impactor. Particles deposit into different impactor stages according to their aerodynamic diameters,[44] and the mass deposited in each stage is used to calculate the effective MMAD. The observed MMAD values represent particles that could be delivered into the deep lung (2.7−6.7 μm) for

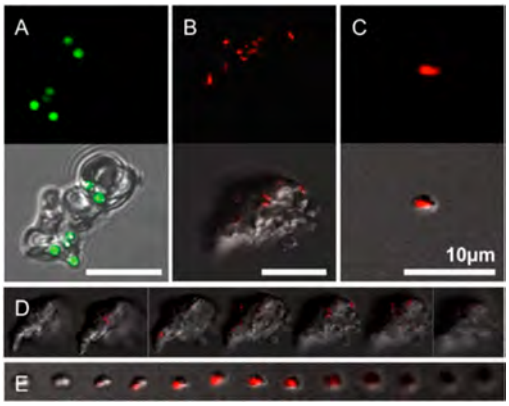

Figure 3. Fluorescence confocal microscopy images of NBCs demonstrate discrete, spray-dried particles that fully encapsulate cells or cell surrogates. (A) Green fluorescent latex beads of 1 μm were used to provide a baseline for spray-dried particles. Encapsulated red fluorescent beads are observed in collapsed merged z-stack images of a typical large (B) and small (C) particle. Particles are shown to fully encapsulate cells as confirmed with three-dimensional z-stack sectioning of the same large (D) and small (E) particle, for which the optical slices are 0.4 and 0.5 μm, respectively, and the total z-scan depths are 13.0 and 6.0 μm, respectively.

all of the processes tested (Table 2). These results indicate that, by variation of the spray-drying conditions, NBCs can be prepared as large particles with high MMADs, small, hollow particles with low MMADs, or a mixed distribution of particles. These size properties could allow for aerosol delivery to the deep lung *via* dry powder inhalation.[16]

Latex Beads and Live Cells Are Incorporated into Spray-Dried NBCs. We characterized NBCs containing encapsulated beads (Figure 3A) and *E. coli* (Figure 3B–E) with confocal microscopy to determine the spatial distribution of cells (or beads) within the dried lipid–silica particles. Shown are representative large particles containing multiple beads or cells and a small particle containing one cell. To verify the complete encapsulation of cells and to visualize their location within dried powders, we collected a z-stack image series of the large and small particles discussed above. These galleries demonstrate complete encapsulation of cells in both large particles containing many cells with a z-stack depth of 13.0 μm (Figure 3D) and small particles containing individual cells with a z-stack depth of 6.0 μm (Figure 3E). The complete set of images used to compile the above images can be found in Supplemental Figures 4 and 5. To determine the distribution of cells within particles of different aerodynamic sizes, particles were collected from each well after MMAD-size separation *via* cascade impaction and imaged with confocal microscopy. We found cells across all of the wells from the largest to the smallest, indicating that particles with MMADs as small as 0.54 μm contain cells (Supplemental Figure 3B), which corresponds to particle sizes that could be delivered to the deep lung.[16]

We extended the spray-drying process to a eukaryotic cell line by encapsulating yeast within lipid–silica NBCs. Fluorescence microscopy images of green-stained cells indicate a dense cell loading within dry powder (Supplemental Figure 6A), and an in-house-developed RNA isolation assay suggests that yeast maintain intact, purifiable RNA within the encapsulated state (Supplemental Figure 6B).

Ubiquitous Nanostructure Extends throughout the Particle, Is Independent of Spray Parameters, and Interfaces Directly with Encapsulated Cell Walls. In the first demonstration of lipid–silica cell encapsulation *via* CDA, Baca *et al.*[7] observed the formation of a conformal, highly ordered periodic nanostructure that surrounded the cells using TEM analysis. This nanostructure was attributed to EISA in which solvent evaporation drives the self-assembly of a lipid–silica (polysilicic acid) mesophase, whose fluidity and conformity to the cell surface were aided by the room-temperature spin-coating process. Room-temperature aging and progressive condensation of the silica precursor resulted in a hardened nanostructure that served to protect the cell within a hydrophilic matrix that prevented cellular desiccation. Here, we questioned whether the elevated temperature, shorter processing time, and higher Peclet number of spray drying *vis-à-vis* aerosol-assisted EISA or spin-coating would inhibit self-assembly and result in disordered/nonuniform nanostructures. In order to examine and characterize the nanostructure of spray-dried powders, we performed low-angle XRD and TEM. The XRD samples were prepared simply by loading dry powder onto the XRD sample stage and gently leveling with a microscope slide such that the sample plane was normal to the stage surface. TEM samples were embedded in epoxy and ultramicrotomed into 60–80 nm thick slices following standard procedures.

Representative XRD patterns are shown in Supplemental Figure 7 and summarized in Table 2 for samples prepared by processes A–E. For all samples, we observe essentially identical, sharp diffraction peaks centered between 2.85 and 2.92°2θ, corresponding to a consistent nanostructure with lattice *d*-spacing $\cong$ 2.3 nm according to Bragg's law. This finding indicates that spray drying yields particles with a well-defined nanostructure that is independent of spraying conditions. For comparison, we also prepared lipid–silica thin films, thick films, and particles from the same precursor sols used in spray drying by spin-coating, casting, or aerosol-assisted EISA, respectively, according to published protocols.[7,35] Both films and aerosol-assisted EISA particles are observed to have prominent low-angle X-ray diffraction peaks (see Supplemental Figure 7). For films, which are processed at room temperature and have a longer drying time (minutes *versus* seconds), we observe the XRD peak to be narrower and shifted to higher 2θ (3.0–3.3° *versus* 2.9°), corresponding to a decrease in *d*-spacing from

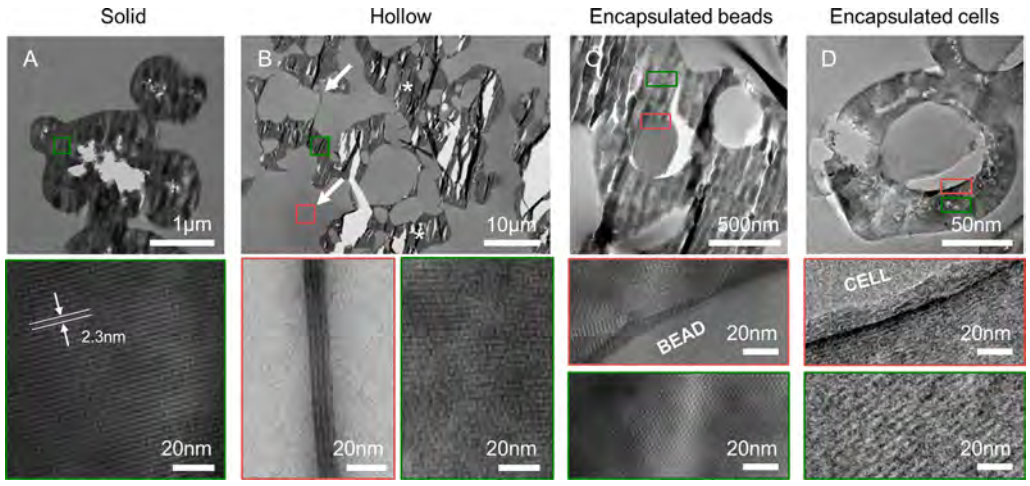

Figure 4. Transmission electron microscopy (TEM) analysis of NBCs reveals that particles possess ubiquitous nanostructure that is independent of the spray-drying parameters and extends throughout solid and hollow regions. (A) Typical particle from a sample prepared according to process A with 60 °C inlet temperature and 3.5 mL/min feed rate having a well-defined nanostructure that extends throughout the bulk of the particle (bottom). (B) Group of particles prepared according to process D with 90 °C inlet temperature and 2.5 mL/min feed rate including a cluster of solid (stars) and hollow particles (arrows). The previously observed nanostructure is found within the perimeter of the hollow shells (bottom, red) and extends into solid regions (bottom, green). (C) NBCs prepared with latex beads, which appear dark gray and are fully encapsulated by a surrounding particle. Zoomed images show nanostructure throughout the bulk of the particle (bottom, green) and interfacing directly with the bead surface (bottom, red). (D) Spray-dried particles containing *E. coli* prepared for TEM following the same technique as with spray-dried beads, which are found to have similar bulk nanostructure (bottom, green) that interfaces coherently with the cell (bottom, red). *E. coli* are stained prior to spray drying with electron-dense osmium tetroxide, which binds to the lipids within the bacterial membrane, providing contrast within the electron beam as compared against the unstained bead interface in (C).

2.3 nm to 2.0 nm. For aerosol-assisted EISA particles, we observe a low-angle X-ray diffraction peak at ~3.0°. We attribute these trends to combined thermodynamic and kinetic effects due to the elevated processing temperature, rapid drying and solidification rate, and high Pe associated with spray drying compared to aerosol-assisted EISA, spin-coating, or casting.

Consistent with the XRD results, TEM imaging of thin sections showed a ubiquitous ordered nanostructure that extends throughout the particle and is independent of spray-drying parameters and particle macromorphology (Figure 4). Samples containing a homogeneous distribution of solid particles (Figure 4A, top) or a mixed distribution of solid and hollow particles (Figure 4B, top) were found to exhibit a highly ordered nanostructure extending throughout the solid regions (Figure 4B, bottom, green) and hollow shells (Figure 4B, bottom, red). The lattice *d*-spacing determined by direct measurement of center-to-center dimensions of the ordered nanostructure is ~2.3 nm and is consistent with the XRD results. We observe both stripe patterns and hexagonally close-packed arrays (Figure 4A–D, lower panels), which we interpret as two different orientations of a hexagonal mesophase, as expected for the short chain diC_6PC lipid due to its low packing parameter, *g*, of 1.5–1.[45] However, we cannot rule out regions of lamellar mesophases. The "chattering" of the microtome cuts evident at lower magnification (Figure 4, top panels, especially in C) is attributed to the unexpectedly high modulus and hardness of the lipid silica mesophase *vide infra*. For samples containing either control latex beads or *E. coli*, we observe that the nanostructure is conformal to the surface of the encapsulated object and extends throughout the particle (Figure 4C and D). Although the disparate hardnesses of the soft cells *versus* the hardened nanostructure make it hard to preserve intact complete cells in the microtomed samples, we located the cell/nanostructure interface by treating cells prior to spray drying with osmium tetroxide (OsO_4), which stains the cell membrane with a high Z contrast agent. Figure 4D highlights the dark rim of the electron-dense OsO_4, which is suggestive of an original conformal nanostructure/cellular interface. Due to the sample thickness, the ordered region within the dark rim is attributed to the deeper lying nanostructure that conformed to the 3D cellular interface.

Here, the ubiquity and uniformity of the nanostructure across all processing conditions could be viewed as surprising given the previous literature indicating that the texture (nanostructure) should depend sensitively on the relative rates of evaporation, solidification, and self-assembly.[25] As we previously reported, the lipid/silica composition is distinguished from typical surfactant or block copolymer-templated mesostructured silica in that the lipid head groups interact through phosphorus with the silicic acid precursors to further reduce the silica condensation rate below that achieved under acidic conditions alone.[46] During EISA, we propose that the reduced condensation rate

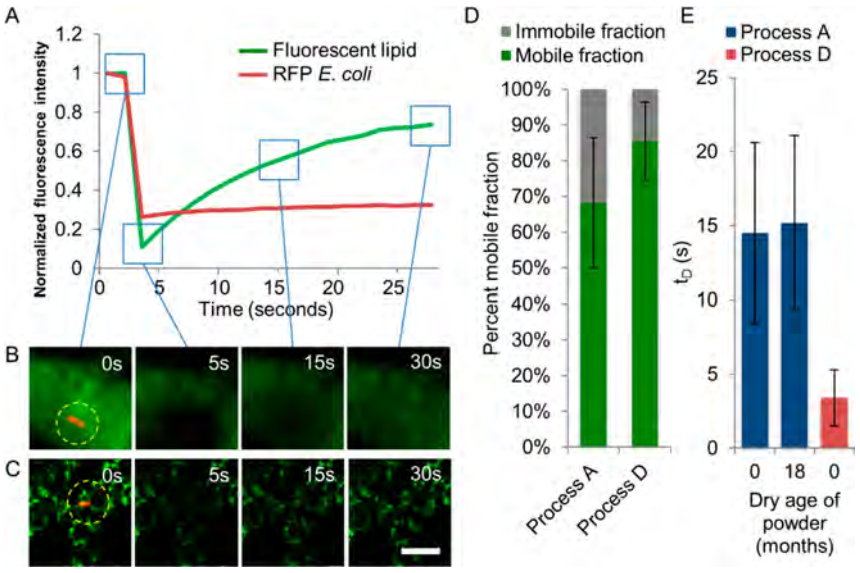

Figure 5. Fluorescence recovery after photobleaching of NBCs prepared with 1% fluorescent lipid (w/w of total lipid fraction) reveals a fluid lipid layer that extends throughout the bulk of the particle that is independent of process parameters and retains fluidity for >18 months. (A) Representative recovery curve showing the recovery profile of a particle prepared under process A. (B, C) Fluorescence recovery image series of regions that were bleached on a large particle from process A (B) and many small particles from process D (C). The green channel exhibits a noticeable recovery, whereas the red channel remains quenched as expected. The particles containing cells exhibit high initial fluorescence in both green (fluorescent lipid) and red (RFP) channels, and both channels are nearly fully quenched after bleaching with a high-intensity laser (yellow dotted circle). The scale bar is 5 μm. (D) Mobile and immobile fractions indicate that 70−85% of the fluorescent molecules are in the mobile phase and contribute to the fluorescence recovery. (E) Lipid recovery is observed by tracking the diffusion time, t_D, the time to recover of half the final recovered fluorescent intensity.

lowers the rate of solidification and minimizes kinetic constraints on self-assembly, explaining the insensitivity of the nanostructure to the spray-drying conditions.

NBCs Incorporate Lipids within an Ordered Nanostructure That Maintains Lipid Fluidity for Periods up to 18 Months under Dry Storage. The role of phospholipids during formation and storage of NBCs is several-fold. First, during CDA they direct the formation of a coherent, fluid (liquid crystalline) lipid−silica mesophase that surrounds the cells and is expected to serve as a biocompatible interface that protects them from osmotic, electrostatic, hydrogen-bonding, and drying stresses during solvent drying. Second, the uniform hydrophilic nature of the nanostructured lipid−silica mesophase is expected to retain water *via* capillary condensation or solvation and thereby prevent cellular desiccation. Third, the nanostructured lipid−silica composite after room-temperature aging and further condensation of the silica framework is envisioned to result in a hard mechanical protective shell for the cells that, by virtue of its internal nanostructure, also provides fluid/molecular accessibility to the cell surface. In order to assess the physicochemical state of the lipid fraction during long-term storage, we performed fluorescence recovery after photobleaching (FRAP), a process in which fluorescent molecules (here, 1% w/w fluorescently labeled lipids of total lipid fraction) within a small 3D disc-shaped volume are quenched (photobleached) with a high-intensity laser pulse and then the region is monitored for fluorescence recovery of intact fluorescent molecules from outside the quenching volume that diffuse into the bleached region (referred to as the mobile fraction). This technique is typically used to characterize membrane component fluidity/diffusivity in cell membranes or lipid vesicles.[47] Analysis of the recovery (shown in Figure 5A is a typical recovery curve) yields the mobile and immobile fractions of the fluorescent population, which are governed by the equation

$$R = (F_\infty - F_0)/(F_i - F_0) \quad (1)$$

where R is the mobile fraction and F is the fluorescence intensity after full bleaching (F_∞), just after bleaching (F_0), and just before bleaching (F_i). FRAP analysis also yields the diffusion time, t_D, defined as the time to recover half the final recovered fluorescent intensity after photobleaching. This is used to calculate the effective diffusion coefficient, D_{eff}, which, for a 2D system, is defined as

$$t_D = \frac{\omega^2 \gamma}{4D_{eff}} \quad (2)$$

where ω is defined as the beam radius and γ is a correction factor for autobleaching in the field of view.[47]

NBCs containing green fluorescent lipid were prepared according to process A, which yields larger, more solid particles (Figure 5B), or process D, which produces smaller, more hollow particles (Figure 5C), and were suspended in PBS and imaged on a Zeiss LSM 510

confocal microscope. A small region containing a cell was chosen, full laser intensity was applied to a circular bleaching region for ~2 s, and both red (cell) and green (lipid) fluorescence channels were monitored until the percentage of fluorescence recovery became approximately constant. Figure 5A is a representative recovery graph for a fresh sample prepared by process A with red and green fluorescence normalized and corrected for photobleaching. Figure 5B and C are image progressions of the process before bleaching (0 s), after bleaching (5 s), after half recovery (15 s), and after full recovery (30 s) for particles made from process A and process D, respectively (bleaching occurred at ~2 s). For process A, we found the mobile and immobile fractions to be 68 ± 18% and 32 ± 18%, respectively, and for process D, we found the mobile and immobile fractions to be 86 ± 11% and 14 ± 11%, respectively (Figure 5D). These values indicate that the majority of the fluorescent species are in the mobile phase and will contribute to fluorescence recovery.

The recovery data were then analyzed for diffusion time in order to determine the diffusion coefficient. We found that the lipid fraction of freshly prepared NBCs recovered to half of the initial fluorescence intensity within 14.5 ± 6.1 and 3.4 ± 1.9 s after bleaching for processes A and D, respectively. Assuming a 2D diffusion model, these values correspond to diffusion coefficients of 0.23 ± 0.04 and 0.8 ± 0.3 $\mu m^2\ s^{-1}$ for processes A and D, respectively. Red cellular fluorescence was fully quenched and did not recover due to the lack of a source of fresh fluorescent species. We repeated this analysis on samples that were aged for 18 months in a sealed container at RT and found that the dry powders maintain fluidity despite the long-term aging (Figure 5E). The 18-month dry-aged samples were analyzed using the previously described 2D model and found to have a diffusion coefficient of 0.3 ± 0.2 $\mu m^2\ s^{-1}$, statistically similar to the unaged sample. A one-way Anova with *post hoc* Holm−Sidak testing shows that both process A samples (0 and 18 months) are significantly different from the process D sample ($p < 0.001$) but are not significantly different from each other.

Overall these results point out that the lipid fraction confined within ordered nanochannels (as observed in Figure 4) retains fluidity and large-scale, effectively three-dimensional fluidic connectivity as required for fluorescence recovery, which involves lipid diffusion over micrometer length scales. The calculated diffusion coefficients are considerably lower than the diffusion coefficients of green fluorescent protein (GFP) in water reported by Potma *et al.* (87 ± 2 $\mu m^2\ s^{-1}$)[48] and GFP in the cytoplasm of *E. coli* reported by Mullineaux *et al.* (9.0 ± 2.1 $\mu m^2\ s^{-1}$);[49] however these are three-dimensional systems and were analyzed using three-dimensional models, whereas our data were analyzed using a two-dimensional diffusion model (*i.e.*, appropriate for vesicles or supported lipid bilayers). A more appropriate comparison would be for GFP in *E. coli* periplasm (D_{eff} = 2.6 ± 1.2 $\mu m^2\ s^{-1}$) and GFP fused to an *E. coli* plasma membrane protein (D_{eff} = 0.13 ± 0.03 $\mu m^2\ s^{-1}$) reported by Mullineaux *et al.*[49] Our observed D_{eff} of green fluorescent lipids in the NBC matrix (0.23 ± 0.04 $\mu m^2\ s^{-1}$) is similar to that reported in the plasma membrane. However, if the hexagonal silica nanostructure confines the lipid as expected from TEM (Figure 4), the diffusion is in fact quasi-one-dimensional and thereby not strictly Brownian.

Nanoindentation Reveals NBCs to Have Modulus and Hardness Properties Exceeding Mesoporous and Biological Silica Materials. Our analysis of NBC nanostructure with TEM required extensive sample preparation and thin-section preparation with microtoming. Over the course of these experiments, we observed distinct blade fatigue and hypothesized that the spray-dried particles were appreciably hard and tough, especially considering the high lipid content and low-temperature processing conditions during sample preparation. To test this hypothesis, we performed nanoindentation on NBCs embedded within an epoxy resin. We used the adjoining surface from which the TEM thin films were microtomed, which takes the shape of a conical frustum (*i.e.*, a cone with its cap removed) (Supplemental Figure 8A). The sample was imaged with SEM in backscatter mode (Supplemental Figure 8B) with no surface modification to visualize the surface distribution of particles within the epoxy resin. NBCs appear white and are clearly distinguishable from the epoxy surroundings (dark gray). Using the same sample, we performed nanoindentation on several particles from different regions on the ~1 mm^2 surface of the substrate (Figure 6). Shown is a typical particle before (Figure 6A and B) and after (Figure 6C) indentation. Indents are marked with black arrows, and the diamond-shaped indenting tip is clearly visualized upon magnification (inset). The NBCs were found to have a Young's modulus of 13.0 ± 1.0 GPa and a hardness of 1.4 ± 0.1 GPa (n = 10). These values are significantly greater than those of an epoxy resin embedding matrix (4.1 ± 0.8 and 0.3 ± 0.1 GPa, respectively). Because indents were individually placed on the NBC particles, we were able to keep the plastic zone within the particle for the hardness measurement, meaning it should be accurate without a matrix effect. The volume of elastically deformed material is greater for the modulus measurement, and we do not know for sure if the elastically deformed region was contained within the NBC or if we were also sampling the epoxy. Therefore, the modulus values we report should be considered to be a lower bound.

Table 3 compares the Young's modulus and hardness of NBCs to other silicate and biocomposite

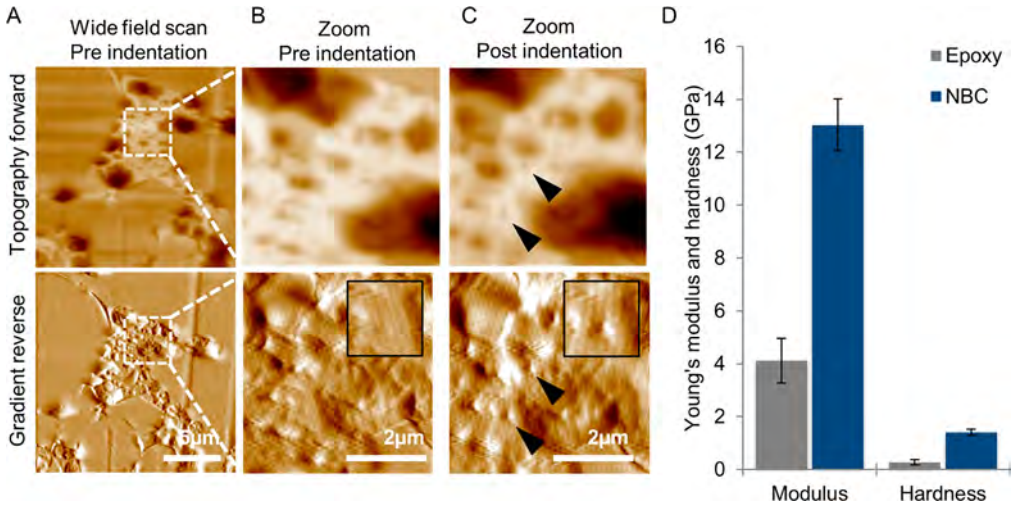

Figure 6. Young's modulus and hardness of NBCs determined by nanoindentation are 13.0 ± 1.0 GPa and 1.4 ± 0.1 GPa, respectively (n = 10), using the standard Oliver−Pharr analysis.[50] The epoxy-embedded sample from which TEM samples were previously microtomed was used to perform indentation studies, as described in Supplemental Figure 8. Nanoindentation was performed using a Hysitron TriboIndenter with a three-sided pyramidal Berkovich tip with 50 nm radius. Pictured are topography images (A−C) achieved by scanning the nanoindentor tip (top) and "gradient reverse" images based on the derivative of the topography image (bottom) of one particle prepared by process A before indentation (wide field scan, left; zoom, center) and after 2× indentations (right). The insets show a typical area before and after indentation. Indentations were taken on multiple particles from different regions of the sample. (D) Young's modulus and hardness of silica NBCs compared to surrounding epoxy (n = 10 and 29, respectively).

TABLE 3. Young's Modulus of NBCs As Compared to Natural and Synthetic Amorphous Silica and Composite Materials

material	Young's modulus (GPa)	hardness (GPa)	ref
nano-biocomposites	13.0 ± 1.0	1.4 ± 0.1	our study
CDA thick films, fresh	4.3 ± 0.1	0.250 ± 0.010	our study
CDA thick films, aged 10 days at 25 °C	4.4 ± 0.1	0.320 ± 0.010	our study
CDA thick films, aged 15 days at 40 °C	4.3 ± 0.2	0.520 ± 0.020	our study
diatom amorphous silica frustules	0.347−2.768	0.033−0.12	Subhash 2005[52]
mesoporous silica (calcined at 500 °C)	10−20	not reported	Fan 2007[51]
dehydrated cortical bone	21.9 ± 3.8	0.79 ± 0.19	Isaksson 2010[53]
	20.02 ± 0.27	not reported	Turner 1999[54]
ultrahigh performance concrete	48.4	not reported	Sorelli 2008[55]
fused silica glass	69.64	9.22	Oliver 2004[50]
nacre aragonite tablets	92	11	Bruet 2005[56]

materials including a hexagonally ordered and oriented 4.5 μm thick cast film prepared from the identical precursor sol as NBCs using the cell directed assembly methodology (see Supplemental Figure 7 for XRD and grazing incidence small-angle X-ray scattering (GISAXS) data). We observe that, despite the mild processing conditions, spray-dried NBCs have Young's modulus and hardness values exceeding those of biological silica, mesoporous silica films, and thick-cast lipid/silica films. Compared to the CDA thick-cast lipid/silica films, whose nearly identical hexagonal mesophase is oriented parallel to the substrate and transverse to the indentation direction, we attribute the appreciably higher modulus of spray-dried samples to the overall 3D orientation of the hexagonal mesophase imposed by confinement of EISA within an evaporating spherical droplet and higher processing temperature, which could promote more extensive silica condensation. With respect to mesophase orientation, we previously showed cubic mesoporous silica films whose mesopore axes were aligned both parallel and perpendicular to the indentation direction to have a higher Young's modulus than hexagonal mesophase films of comparable density whose pore axes were aligned perpendicular to the indentation direction.[51] With respect to potential effects of more extensive condensation on mechanical properties, we determined that room-temperature aging for 10 days or 40 °C aging for 15 days resulted in significantly increased hardness (320 and 520 MPa, respectively, *versus* 250 MPa for unaged samples), while having no significant effect on the Young's modulus, which remained ~4.3 GPa. These values remain considerably lower than for the spray-dried NBC materials.

NBC Encapsulation Induces a Viable but Not Culturable State. The Young's modulus of *E. coli* has recently been

determined to be ~30 MPa,[57] which is approximately 500-fold lower than that of its surrounding lipid−silica nanostructure within NBCs. Thus, the encased bacteria will be physically locked in place within the nanostructure and unable to grow. There is also the potential that the more rigid NBC nanostructure could exert significant mechanical stress upon the bacteria during spray drying, where capillary (drying) stresses and continued condensation of the silica framework would impose compressive stresses on the cells.[3] We hypothesized that this profound three-dimensional mechanical constraint might induce unique physiological responses in the encased bacteria. It has been shown that a complex relationship exists between mechanical stress and the viable but not culturable (VBNC) state: VBNC can be induced by mechanical stresses such as high pressure,[58] while a pre-existing VBNC state can cause resistance to mechanical stress-induced killing.[59] Our own studies of cellular encapsulation of bacterial cells[3] have consistently shown poor viability of encapsulated bacteria unless they were first incubated in nutrient-free salt solutions such as PBS that are known to induce VBNC through starvation. This observation is consistent with the idea that NBC-encapsulated bacteria could be forced into a VBNC state, enabling preinduced VBNC cells to better survive encapsulation. Two key parameters define the VBNC state: (i) extended retention of markers of cellular metabolism and viability such as ATP levels together with (ii) a failure to grow on the routine bacteriological media in which they would normally grow and develop into colonies.[60]

To assess cellular viability, we used a luminescence-based adenosine triphosphate (ATP) assay, which is a well-known surrogate indicator for cellular metabolism and viability[61,62] and has been used in similar live-cell biomaterial research.[63] In this process, ATP is quantified through the ATP-enabled conversion of beetle luciferin to oxyluciferin by firefly luciferase, resulting in a luminescent signal, which is analyzed on a luminometer and is directly proportional to the amount of ATP present. NBCs were prepared as described according to process A and were stored according to published standards on aging of drug and vaccine formulations[64] at 4 °C (RH% not specified), 25 °C/60% RH, 40 °C/75% RH, or 40 °C/0% RH. At higher temperatures and humidities, bacterial metabolism will be increased, and, in the absence of any nutrients or any ability to benefit from other dead, hydrolyzed cell components (the NBC cells are physically isolated from one another and have limited intracellular diffusivity), we would expect viability and ATP levels of VBNC cells to decrease, as is generally observed for cell-based vaccines and other medical products. We analyzed NBC samples periodically for up to 8 months and found a strong relationship between ATP retention, time and storage conditions (Figure 7). For samples stored at 0% RH, ATP loss was minimal after 8 months, whereas it decreased markedly at 25 °C/60% RH and 40 °C/75% RH. Samples stored at 4 °C were analyzed only at the beginning and at end of the experiment due to experimental limitations and showed negligible ATP loss after 8 months (Supplemental Figure 9D).

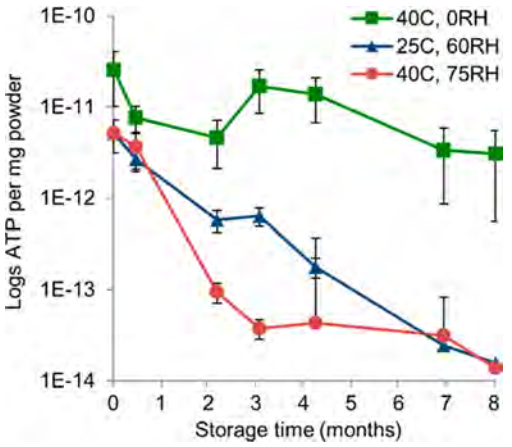

Figure 7. An ATP-based viability assay of aged NBCs indicates that encapsulated cells are viable for >8 months with less than 1-$\log_{10}$ loss in ATP for samples stored at 40 °C and 0% relative humidity (RH) and that this long-term viability is independent of process parameters. Spray-dried samples were prepared, split into 5−10 mg aliquots, and stored at 25 °C/60%RH, 40 °C/75%RH, and 40 °C/0%RH. Samples were periodically removed from aging and resuspended in water to a 25 μL/mg dilution. The solution was thoroughly mixed, and 25 μL was added to a 96-well plate in duplicate. The luciferase reagent was prepared according to product literature, 50 μL of reagent was added to each sample well, and the plate was analyzed on a Tecan luminometer. The data were normalized to ATP standards and converted to moles of ATP. For samples stored at 40 °C and 0%RH, we observed <1-$\log_{10}$ loss in viability after 8-months aging, a significant improvement over reported values of ~4-$\log_{10}$ loss of viability during storage under the same conditions for only 30 days (Supplemental Figure 9).

To determine the effect of sample preparation conditions on ATP, we prepared samples using different spraying parameters described in Table 2 and measured ATP levels as a function of aging at 40 °C/75RH or 40 °C/0RH. For all processes listed, ATP levels decreased similarly to process A (Supplemental Table 1). These findings demonstrate the physiological modulation caused by NBC encapsulation is independent of spraying conditions. Spray-dried biomaterials are often prepared with excipient materials such as trehalose,[10] sucrose,[11] and leucine[12] to reduce cell death resulting from osmotic and drying stresses. We prepared NBCs according to process A and included 15 or 100 mM of each excipient separately from the precursors before spraying. Samples were stored for 2 months at 40 °C/75RH and analyzed for ATP. All samples behaved similarly, losing between 2.7 and 3.1 logs ATP (Supplemental Table 2) and so do not improve upon losses observed for control samples (no excipient). This suggests that the progressive replacement of water with the conformal, hydrophilic lipid−silica nanostructure (Figure 4) during spray

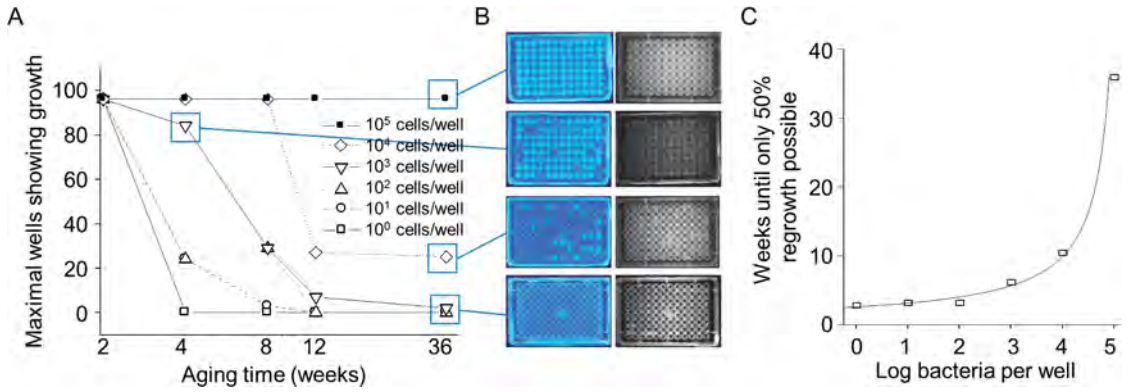

Figure 8. Dry-aged encapsulated cells can be regrown in liquid culture and demonstrate some characteristics of bacterial persistence. Here, the same, known concentration of NBC-encapsulated cells is added to each well of a 96-well plate, and the plate is sealed and incubated with shaking for up to 2 months. If it occurs, the growth in a well takes <24 h to go from null to maximal growth and is observed by monitoring RFP bacterial fluorescence. The majority of growth occurs within the first several days of incubation, but it can continue for up to 2 weeks, after which point little growth was observed. (A) Number of wells showing regrowth after dry aging of encapsulated cells for up to 36 weeks prior to incubation. (B) Representative fluorescence images taken with a digital camera with backlighting from a UV-transilluminator (blue) and a fluorescent plate reader (black and white) of 96-well plates that were used to conduct the experiment, highlight wells that exhibit growth (bright wells). (C) Maximum weeks of aging where 50% regrowth/resuscitation remains possible as a function of the average number of cells/well.

drying maintains a biocompatible nano/biointerface. Furthermore, the addition of liquid growth media to spray-dried NBCs resulted in a noticeably greater decline in ATP with a loss of 3.8 logs ATP after 2 months (Supplemental Table 2). A similar behavior was described by Harper *et al.*[3] and was attributed to the effects of increased metabolism of encapsulated cells and resulting decreased ability to cope with stresses of cellular confinement. Induction of a VBNC state by physical and chemical cellular confinement within a rigid biocompatible nanostructure is consistent with our observations.

In addition to sustained ATP levels, the VBNC state is characterized by a significant reduction in the ability of the VBNC cells to enter back into normal cell growth and division, a process termed resuscitation.[65] However, quantifying the numbers of VBNC cells capable of resuscitation can be challenging. Although plating on solid media allows for colony counting from isolated progenitor VBNC cells, many bacteria show much less ability to grow from such states on solid media compared to liquid media, exemplified by *Mycobacterium tuberculosis*, which is capable of extended VBNC or latency.[66] We hypothesized that NBCs could provide a model of VBNC bacteria, and their resuscitation would enable temporal separation of the VBNC state and subsequent resuscitation states. In our model, the VBNC state occurs in the solid phase encapsulating matrix, and resuscitation then occurs in liquid phase culture after dissolution of the silica.[3] To test this hypothesis, we measured the frequency of cellular resuscitation in media after increasing periods in the NBC-induced VBNC state. *E. coli* expressing RFP were spray-dried and aged at room temperature and humidity for 0 to 36 weeks. The total number of cells spray-dried was divided by the total collected amount of powder to yield an approximate cell-loading quantity. Aliquots of NBC with an estimated specific cell count were then serially diluted in PBS containing 20% fetal bovine serum (FBS) and dispensed in 96-well plates so that each well would contain the same average number of cells. Dilutions ranged from 10^0 to 10^5 cells/well/plate. Plates were capped, sealed with adhesive tape to prevent evaporation, and incubated at 37 °C with moderate rotary agitation for 8 weeks. Plates were analyzed periodically during the course of liquid incubation for bacterial fluorescence from RFP, which indicates regrowth (resuscitation), using a fluorescence plate-reader and, for visual confirmation, a digital camera and UV-transilluminator. Figure 8A and B show the regrowth results after 56 days of liquid incubation (number of wells of a 96-well plate showing regrowth) as a function of dry aging time of the encapsulated cells under ambient conditions. Supplemental Figure 9C shows a time course of resuscitation for samples aged for 2 weeks and dispensed at a concentration of 100 cells per well. We observe resuscitation to occur rapidly and nearly completely. This level of resuscitation correlates well with the ~96% viability of *E. coli* immediately prior to encapsulation as determined with live/dead staining (Supplemental Figure 9A and B). Regrowth occurred in wells in a rapid, but stochastic manner and was consistent with a control experiment in which overnight growth of a single cell led to a positive signal. Thus, resuscitation of a single cell from the VBNC state to growth is sufficient to result in overnight growth to turbidity and a positive RFP signal. The frequency of this resuscitation event can then be determined from its occurrence as a function of total initial colony forming units (CFU)

added; low-frequency resuscitation will be apparent only at high CFUs per well. The number of wells exhibiting regrowth as a function of CFU and liquid incubation time is shown for NBC aging times of 0−36 weeks in Figure 8. It can be seen that the frequency of resuscitation decreased with the time in the VBNC state. Supplementary Figure 10A−F demonstrate that, generally, resuscitation occurred in the first few days of liquid media incubation. However, Supplemental Figure 10D−F show that at greater periods of NBC-induced VBNC resuscitation could take up to 4 weeks of liquid culture to achieve maximal resuscitation. (The frequency of such late resuscitation events was low, as it was only observed for $>10^3$ CFU/well.)

Figure 8A shows the maximal number of wells showing growth (after 56 days of liquid media culture) as a function of time of NBC aging (under ambient conditions prior to introduction to media). Representative digital images and plate reader images of plate growth are shown in Figure 8B. As the aging time increased, the number of wells exhibiting resuscitation and growth decreased in a concentration-dependent manner, where lower cells/well reduced the ability for resuscitation in any well. At greater cells/well, the probability of a resuscitation event increased and was possible even after extended periods of NBC aging. The fraction of at least 50% of the wells undergoing resuscitation as a function of aging time and initial CFU is shown in Figure 8C, demonstrating that the frequency of resuscitation after periods of time of aging exceeding about 10 weeks is rare (less than 1 in 10^4 cells).

Combined, the high preservation of cellular ATP but very low frequency of resuscitation of NBC-encapsulated bacteria is consistent with a large population in the VBNC state. This approach enables the determination of resuscitation probabilities from VBNC using a high-throughput platform even when such events are rare. As well as enabling basic studies of bacterial resuscitation, this platform could also be used to study important relevant characteristics of the VBNC state such as gene or protein expression and to screen drugs that are capable of killing these rare and persistent cells, which are relevant to bacterial diseases such as tuberculosis (TB) that can cause latent infection. Furthermore, latent TB is the dominant form of the disease and a target for latency-specific live cell vaccine development. Since VBNC cells in this platform will mimic the latent state, specific overexpression of latency-associated antigens by these cells might improve the efficacy of such latency-targeted vaccines.

CONCLUSION

The field of live cell encapsulation within solid-state materials is rapidly growing with the potential for many important applications within biomaterial and biomedical research. Here, we have introduced a new technique that extends the process of cell-directed assembly with sol gel nanomaterials by using a spray-drying approach for the scalable production of lipid−silica nano-biocomposite biomaterials with fully encapsulated, live cells. The spraying conditions offer brief cell−solvent contact times, low operating temperatures, and rapid droplet drying rates, allowing for cell viability in otherwise harsh material preparation conditions. The NBCs are found to have a highly ordered nanostructure independent of spray-dry conditions incorporating a fluid lipid interphase that is retained after 1.5 years of storage at room temperature, yet they are extraordinarily rigid, exhibiting a Young's modulus of 13 GPa and a hardness of 1.4 GPa. These unique properties appear to induce the VBNC state, although resuscitation from the persistent state is possible after even extended periods. The materials provide a model for determining VBNC resuscitation frequencies across a wide range of variation. While viability and nanostructure appear independent of spray-drying parameters, particle macromorphology, density, and aerodynamic diameters were variable through systematic control of the processing parameters. Such particles, through their enhanced expression of VBNC-related antigens, could prove useful in the development of live vaccines against diseases in which the VBNC state may be clinically important, such as latent tuberculosis.

MATERIALS AND METHODS

Materials. Leucine, trehalose, carbenicillin disodium salt, Lennox broth (LB), agar, acetonitrile, ethanol (absolute), tetraethyl orthosilicate, and hydrochloric acid were purchased from Sigma-Aldrich. Short-chain 1,2-dihexanoyl-*sn*-glycero-3-phosphocholine (*di*C_6PC) and 1-hexanoyl-2-{6-[(7-nitro-2-(1,3-benzoxadiazol)-4-yl)amino]hexanoyl}-*sn*-glycero-3-phosphocholine (06:0−06:0 NBD PC) were obtained from Avanti Polar Lipids (Alabaster, AL, USA). Fluorescent biomarker SYTO 9 green fluorescent permeable nucleic acid stain was obtained from Invitrogen (now part of Life Technologies, Carlsbad, CA, USA). Fluoromax fluorescent latex beads (1 μm) were obtained from Thermo Scientific. Nitrogen (N_2) was purchased from a local supplier (Argyle Gas, Albuquerque, NM, USA).

Cell Culture. Bacteria (K12 *Escherichia coli,* strain BL21) was purchased from Sigma-Aldrich and transformed with pDsRed-Express 2 (Clontech, Mountain View, CA, USA), which constitutively expresses DSRed-Express2, a highly stable red fluorescence protein variant, and confers resistance to ampicillin or carbenicillin for cell selection. Cells were grown in LB (20 g/L) containing 100 μg/mL carbenicillin for 12 h at 37 °C with shaking until an OD_{600} of 1.2−1.5 was reached, and the cells were washed three times by pelleting at 4000 rpm for 5 min and resuspended in PBS. All cell-culturing materials were ordered from Sigma including PBS, LB, carbenicillin, and FBS.

Silica Precursors and Precursor Sol. Prehydrolyzed tetraethyl orthosilicate stock solutions (A2**) were prepared following previously used methods[7] by refluxing 61 mL of TEOS, 61 mL of

ethanol, 4.9 mL of DI water, and 0.2 mL of 0.07 N HCl (molar ratio 1:4:1:5 $\times$ 10^{-5}) for 90 min at 60 °C. Stock solutions were stored at −20 °C. The silica precursor sol was prepared by adding 0.83 mL of A2** stock to a solution containing 1.33 mL of DI water, 0.66 mL of ethanol, and 0.53 mL of 0.07 N HCl. This solution was homogenized with mild agitation followed by aging at room temperature on a rocking platform for 30−60 min (see Supplemental Figure 1). Immediately prior to spray drying, 100 mg of lipid was added to the aged precursor solution and mixed until fully dissolved (~20 s). This is the final, active lipid−silica precursor solution that we refer to as precursor sol.

Preparation and Storage of Spray-Dried NBCs and Thin-Film Analogues. Samples were spray-dried with a B-290 mini spray drier (Büchi, Flawil, Switzerland) using a 0.7 mm nozzle. Initial spray-drying parameters were based on protocols used in similar live-cell spray drying, although we increased the pump speed to minimize cell contact with the acidic and alcoholic precursor sol.[19] These initial processing conditions were defined as process A and consisted of a 60 °C inlet temperature, 90% aspiration rate, 3.5 mL/min peristaltic pump feed rate, and 60 L/h nitrogen carrier gas rate. A 3.3 mL amount of precursor sol and 3.3 mL of cells in liquid suspension were loaded into separate scintillation vials. Two peristaltic pumps with a combined feed rate of 3.5 mL/min were used to deliver the solutions to the nozzle with mixing *via* a Y connector immediately prior to aspiration into the nozzle. Spray-dried particles were collected in scintillation vials that were connected to the standard cyclone with a custom-built adapter, replacing the standard collection chamber. Sample yields were approximately 100−150 mg per batch, corresponding to approximately (1.0−1.5) $\times$ 10^7 cells/mg powder. This collection variability is dependent upon spray-drying parameters, and lower collection yields are attributed to losses of sub-micrometer particles that are removed from the spray-drying assembly by vacuum (Supplementary Figure 2). After spray drying, samples were stored at 4 °C, 25 $\pm$ 2 °C/60 $\pm$ 5%RH, 40 $\pm$ 2 °C/75 $\pm$ 5%RH, or 40 $\pm$ 2 °C/0 $\pm$ 5%RH according to published aging standards.[64]

For comparison to previous studies in CDA,[7] we prepared thin films *via* spin-coating, thick films *via* bulk solution evaporation (casting), and aerosolized samples *via* aerosol-assisted EISA according to published techniques[7,35] (see Supplemental Figures 2 and 7 for experimental details).[7,35]

Characterization of Particle Morphology and Size. To determine the physical structure of NBCs, we analyzed samples prepared under different conditions with varying inlet temperatures and feed rates as described in Table 1 and imaged the samples with SEM, confocal, and TEM. The percentage fraction of hollow particles within a sample was determined by counting >300 particles per sample in SEM images and differentiating between solid and hollow particles.

The hydrodynamic diameter, D_{50}, of dried powders was measured using a Sympatec HELOS laser diffractometer (Clausthal-Zellerfeld, Germany). A 1−2 mg amount of powder was suspended in 1 mL of water, sonicated for 10 s to break up particle agglomerates, and vortexed for 30 s to distribute individual particles, and the vial was left to rest for 60 s to allow additional aggregates to settle out of suspension. A 100 μL amount of suspension was pipetted into the LD cuvette containing 6 mL of acetonitrile and mixed thoroughly, and data were collected. The fine particle fraction mass mean aerodynamic diameter was determined using a Next Generation pharmaceutical cascade impactor (NGI, Copley Scientific Ltd., Nottingham, UK). Powders were dry-injected into the cascade impactor using a DP-4 dry powder insufflator (PennCentury, Wyndmoor, PA, USA) to disperse the individual particles. A pump maintained a steady flow through the NGI to simulate inspiration (30 L/min). We observed some degree of particle clumping during the pressurized aspiration process, which likely caused particles to be forced together, as explained by T. Langrish[33] and is attributed to the large lipid fraction. This behavior was accounted for by subtracting out the weight of the sample that deposited within the largest well of the cascade impactor (well #1), allowing us to sort out large aggregates of particles, which, *in vivo*, would deposit within the upper respiratory tract of the lung. The effective fine particle fraction MMAD value represents the effective size of particles that would be delivered into the deep lung and fell within 2.6−6.8 μm for all of the processes tested (Table 2).

Optical Microscopy. For optical imaging, dried powders were suspended in water, vortexed for 10 s, and pipetted onto standard microscope slides. Samples were imaged on a Zeiss LSM 510 confocal microscope mounted on a Zeiss Axiovert 100 inverted microscope. Latex beads are phosphorescent (excitation and emission peaks are 468 and 508 nm), yeast were stained with Syto-9 green fluorescent dye according to manufacturer's specifications, and *E. coli* samples constitutively express an RFP variant (excitation and emission peaks are 554 and 591 nm) and were not further fluorescently treated. The lipid phase, which extends throughout the particle, was fluorescently labeled by including 1% w/w NBD-labeled C-6 PC lipid with the C-6 lipid prior to addition to precursor sol.

We created z-stack images for particles of varying sizes in order to visualize the distribution of cells within particles. This was achieved by setting the upper and lower boundaries of a particle and taking an image with a given optical slice diameter (here 0.4 and 0.5 μm for the large and small particle in Figure 3 and in Supplemental Figures 4 and 5) and collecting an image every diameter distance. The resulting collection of images maps the entire z-dimension within the sample, allowing us to create 3D reconstructions of the sample.

Electron Microscopy. Scanning electron microscopy was performed using a Hitachi S-5200 Nano SEM operating between 1 and 5 kV. Spray-dried NBCs were distributed onto a SEM sample boat coated in carbon tape and seated into the tape with a short pulse of N_2 gas. No further sample preparation was performed for imaging.

Transmission electron microscopy was performed using a Hitachi H7500 TEM equipped with an AMT XR60 bottom mount camera or on a JEOL 2010F field emission HRTEM/STEM with HAADF detector. NBCs containing beads or *E. coli* were suspended overnight in PBS at 4 °C, fixed in 2.5% glutaraldehyde in PBS overnight at 4 °C, washed three times in PBS, fixed in 1% osmium tetroxide (only for samples containing *E. coli* cells), washed three times in water, dehydrated in a graded ethanol series, and switched to anhydrous acetone for the final dehydration. The preparation was then infiltrated with resin by incubating particles in 1:1 Spurr's resin/acetone, 3:1 Spurr's resin/acetone, and, finally, 100% Spurr's resin. Samples were placed in embedding molds and polymerized by incubation at 60 °C for at least 16 h, and the blocks were trimmed for microtoming. Microtomed sections with thicknesses between 60 and 80 nm were used for imaging.

Measurement of Lipid Fluidity. Fluorescence recovery after photobleaching was used to measure lipid fluidity using the confocal setup as described above. Samples were prepared using process A and D spray-drying methodologies and included 1% w/w NBD-labeled C-6 PC lipid (added to precursor sol along with C-6 lipid). Powders were spray-dried, collected, and resuspended in PBS immediately prior to imaging. FRAP was performed by photobleaching a region on a particle and measuring the following fluorescence recovery. Autobleaching was measured in an adjacent, unbleached region and used as a correction factor for the FRAP recovery data.

Nanoindentation Characterization of NBC Modulus and Hardness. Nanoindentation was performed on a Hysitron TriboIndenter with a cube-corner tip. We used the pyramidal shaped epoxy-resin substrate that was used for the TEM experiments for all nanoindentation experiments. During NBC indentation the contact radius was kept small so that the plastic zone beneath the tip (approximately 3 times contact radius) was contained within the NBC with minimal influence from the epoxy-resin substrate. A fused quartz standard was used to determine the indenter tip area as a function of contact depth. Control indents were performed in the epoxy regions surrounding the encapsulated particles. Young's modulus and hardness for both NBC and epoxy indents were determined *via* the Oliver−Pharr method.[50]

ATP Assay. We used a commercial ATP-based luminescence assay (Bactiter Glo, Promega). After storage under the above-mentioned conditions, a measured amount (5−10 mg) of dry

powder was resuspended in water to a 1 mg/25 μL dilution. The solution was thoroughly mixed, and 25 μL was added to wells in a 96-well plate. The Bactiter reagent was prepared according to product literature, 50 μL of reagent was added to each sample well, and the plate was analyzed on a Tecan luminometer. The data were normalized to ATP standards (containing 10^{-11} to 10^{-16} mol of ATP). The data are representative of four experiments. As a control, encapsulated beads were analyzed and found to be below our limit of detection.

Culturability Assay. NBC samples were freshly prepared, sealed in an airtight vial, and dry aged at RT for 2, 4, 8, 12, and 36 weeks prior to the start of the culturing experiment. At the start of the experiment, 96-well plates were prepared by loading the same weight of powder containing an approximate cell/mg loading as described above into each of the 96 wells in three steps such that each well had the same approximate number of cells. First, we prepared a set of serial dilutions of cells in media. The media used consisted of 20% FBS containing carbenicillin, which we prepared immediately before the experiment. For the cell dilutions, 1.2 mg of NBC was added to 1.2 mL of media (yielding 1 mg/mL), 0.12 mL of this solution was added to 1.08 mL of media (yielding 0.12 mg/1.2 mL $\equiv$ 0.1 mg/mL), and so forth. This dilution set, therefore, consists of NBCs in media with approximately 10^7 cells/mL, 10^6 cells/mL, *etc*. Second, we added the cell/media solution to the 96 wells on a plate. A 1 mL amount of the first dilution containing 10^7 cells/mL was added to 9 mL of media as described above in a small vial. This solution was stirred continuously with a stirplate/stirbar throughout the following preparation to ensure a well-mixed product. A 100 μL amount containing 10^5 cells was pipetted into each well of the first 96-well plate, and the remaining 400 μL was discarded. The plate was then set aside, and the remaining cell dilutions were prepared in the same way. Third, the plate was capped and sealed around the perimeter with adhesive tape to prevent evaporation. This method was shown to contain liquid media for significantly longer than the duration of the experiment (data not shown). The final set of samples were seven 96-well plates containing 10^5 cells/well/plate, 10^4 cells/well/plate, ..., 10^0 cells/well/plate, and a control plate in which we substituted 1 mL of PBS for the 1 mL of cell dilution added to 9 mL of media. The seven plates were sealed in a container as a further prevention against evaporation and incubated at 37 °C/60 rpm for 8 weeks. For analysis, each day for the first week and weekly thereafter, we imaged each plate using a fluorescence plate reader with excitation and emission filters set to DsRed fluorescence (554 and 591 nm, respectively). For visual clarity, we also imaged plates using a digital camera with excitation from a UV-transilluminator. The entire above procedure was then repeated periodically such that regrowth data points occurred at 2, 4, 8, and 32 weeks of dry sample aging.

Conflict of Interest: The authors declare no competing financial interest.

Acknowledgment. We would like to thank Y. B. Jiang for help with TEM sample preparation. Fluorescence images in this paper were generated in the University of New Mexico & Cancer Center Fluorescence Microscopy Shared Resource funded as detailed at http://hsc.unm.edu/crtc/microscopy/acknowledgement.shtml. C.J.B. and E.C. acknowledge support from the U.S. Department of Energy, Office of Science, Basic Energy Sciences, Materials Sciences and Engineering Division, and the Sandia National Laboratory LDRD program. P.E.J. and J.P. acknowledge support from the NSF IGERT program and the Air Force Office of Scientific Research under grant no. FA9550-14-1-0066. Nanoindentation studies were performed at the Center for Integrated Nanotechnologies, an Office of Science User Facility operated for the U.S. Department of Energy (DOE) Office of Science. Los Alamos National Laboratory, an affirmative action equal opportunity employer, is operated by Los Alamos National Security, LLC, for the National Nuclear Security Administration of the U.S. Department of Energy under contract DE-AC52-06NA25396. G.S.T. acknowledges support from NIH/NIAID AI081015 and 081090. C.J.B. and E.C.C. acknowledge support from the U.S. Department of Energy, Office of Science, Basic Energy Sciences, Materials Sciences and Engineering Division for support of self-assembly of lipid-silica nanocomposites, and the Sandia National Laboratory LDRD program for support of studies of cellular function. We thank Patrick Fleig for preparing the aerosol samples shown in Supplemental Figure 2. TEM Data were generated in the UNM Electron Microscopy Shared Facility supported by the University of New Mexico Health Sciences Center and the University of New Mexico Cancer Center.

Supporting Information Available: The Supporting Information is available free of charge on the ACS Publications website at DOI: 10.1021/acsnano.5b01139.

REFERENCES AND NOTES

1. Carturan, G.; Campostrini, R.; Diré, S.; Scardi, V.; De Alteriis, E. Inorganic Gels for Immobilization of Biocatalysts: Inclusion of Invertase-Active Whole Cells of Yeast (Saccharomyces cerevisiae) into Thin Layers of SiO_2 Gel Deposited on Glass Sheets. *J. Mol. Catal.* **1989**, *57*, L13–L16.
2. Nassif, N.; Bouvet, O.; Noelle Rager, M.; Roux, C.; Coradin, T.; Livage, J. Living Bacteria in Silica Gels. *Nat. Mater.* **2002**, *1*, 42–44.
3. Harper, J. C.; Lopez, D. M.; Larkin, E. C.; Economides, M. K.; McIntyre, S. K.; Alam, T. M.; Tartis, M. S.; Werner-Washburne, M.; Brinker, C. J.; Brozik, S. M.; *et al*. Encapsulation of S. cerevisiae in Poly(glycerol) Silicate Derived Matrices: Effect of Matrix Additives and Cell Metabolic Phase on Long-Term Viability and Rate of Gene Expression. *Chem. Mater.* **2011**, *23*, 2555–2564.
4. Wang, B.; Liu, P.; Jiang, W.; Pan, H.; Xu, X.; Tang, R. Yeast Cells with an Artificial Mineral Shell: Protection and Modification of Living Cells by Biomimetic Mineralization. *Angew. Chem., Int. Ed.* **2008**, *47*, 3560–3564.
5. Gupta, G.; Rathod, S. B.; Staggs, K. W.; Ista, L. K.; Oucherif, K. A.; Atanassov, P. B.; Tartis, M. S.; Montãno, G. A.; López, G. P. CVD for the Facile Synthesis of Hybrid Nanobiomaterials Integrating Functional Supramolecular Assemblies. *Langmuir* **2009**, *25*, 13322–13327.
6. Carturan, G.; Dal Toso, R.; Boninsegna, S.; Dal Monte, R. Encapsulation of Functional Cells by Sol-Gel Silica: Actual Progress and Perspectives for Cell Therapy. *J. Mater. Chem.* **2004**, *14*, 2087.
7. Baca, H. K.; Ashley, C.; Carnes, E.; Lopez, D.; Flemming, J.; Dunphy, D.; Singh, S.; Chen, Z.; Liu, N.; Fan, H.; *et al*. Cell-Directed Assembly of Lipid-Silica Nanostructures Providing Extended Cell Viability. *Science* **2006**, *313*, 337–341.
8. Carnes, E. C.; Lopez, D. M.; Donegan, N. P.; Cheung, A.; Gresham, H.; Timmins, G. S.; Brinker, C. J. Confinement-Induced Quorum Sensing of Individual Staphylococcus aureus Bacteria. *Nat. Chem. Biol.* **2010**, *6*, 41–45.
9. Vehring, R. Pharmaceutical Particle Engineering via Spray Drying. *Pharm. Res.* **2008**, *25*, 999–1022.
10. Maury, M.; Murphy, K.; Kumar, S.; Shi, L.; Lee, G. Effects of Process Variables on the Powder Yield of Spray-Dried Trehalose on a Laboratory Spray-Dryer. *Eur. J. Pharm. Biopharm.* **2005**, *59*, 565–573.
11. Tzannis, S. T.; Prestrelski, S. J. Activity-Stability Considerations of Trypsinogen during Spray Drying: Effects of Sucrose. *J. Pharm. Sci.* **1999**, *88*, 351–359.
12. Wong, Y.-L.; Sampson, S.; Germishuizen, W. A.; Goonesekera, S.; Caponetti, G.; Sadoff, J.; Bloom, B. R.; Edwards, D. Drying a Tuberculosis Vaccine without Freezing. *Proc. Natl. Acad. Sci. U.S.A.* **2007**, *104*, 2591–2595.
13. Pilcer, G.; Sebti, T.; Amighi, K. Formulation and Characterization of Lipid-Coated Tobramycin Particles for Dry Powder Inhalation. *Pharm. Res.* **2006**, *23*, 931–940.
14. Sebti, T.; Amighi, K. Preparation and in Vitro Evaluation of Lipidic Carriers and Fillers for Inhalation. *Eur. J. Pharm. Biopharm.* **2006**, *63*, 51–58.
15. Nijdam, J. J.; Langrish, T. A. G. An Investigation of Milk Powders Produced by a Laboratory-Scale Spray Dryer. *Dry. Technol.* **2005**, *23*, 1043–1056.
16. Pulliam, B.; Sung, J. C.; Edwards, D. A. Design of Nanoparticle-Based Dry Powder Pulmonary Vaccines. *Expert Opin. Drug Delivery* **2007**, *4*, 651–663.

17. Edwards, D. A.; Hanes, J.; Caponetti, G.; Hrkach, J.; Ben-Jebria, A.; Eskew, M. L.; Mintzes, J.; Deaver, D.; Lotan, N.; Langer, R. Large Porous Particles for Pulmonary Drug Delivery. *Science* **1997**, *276*, 1868–1871.
18. Edwards, D. A.; Dunbar, C. Bioengineering of Therapeutic Aerosols. *Annu. Rev. Biomed. Eng.* **2002**, *4*, 93–107.
19. Ohtake, S.; Martin, R. A.; Yee, L.; Chen, D.; Kristensen, D. D.; Lechuga-Ballesteros, D.; Truong-Le, V. Heat-Stable Measles Vaccine Produced by Spray Drying. *Vaccine* **2010**, *28*, 1275–1284.
20. Garcia-Contreras, L.; Wong, Y.-L.; Muttil, P.; Padilla, D.; Sadoff, J.; Derousse, J.; Germishuizen, W. A.; Goonesekera, S.; Elbert, K.; Bloom, B. R.; *et al*. Immunization by a Bacterial Aerosol. *Proc. Natl. Acad. Sci. U.S.A.* **2008**, *105*, 4656–4660.
21. Cowan, D. A.; Casanueva, A. Stability of ATP in Antarctic Mineral Soils. *Polar Biol.* **2007**, *30*, 1599–1603.
22. Gottenbos, B. Antimicrobial Effects of Positively Charged Surfaces on Adhering Gram-Positive and Gram-Negative Bacteria. *J. Antimicrob. Chemother.* **2001**, *48*, 7–13.
23. Pope, E. J. A.; Braun, K.; Peterson, C. M. Bioartificial Organs I: Silica Gel Encapsulated Pancreatic Islets for the Treatment of Diabetes Mellitus. *J. Sol-Gel Sci. Technol.* **1997**, *8*, 635–639.
24. Lu, Y.; Fan, H.; Stump, A.; Ward, T. L.; Rieker, T.; Brinker, C. J. Aerosol-Assisted Self-Assembly of Mesostructured Spherical Nanoparticles. *Nature* **1999**, *398*, 223–226.
25. Boissiere, C.; Grosso, D.; Chaumonnot, A.; Nicole, L.; Sanchez, C. Aerosol Route to Functional Nanostructured Inorganic and Hybrid Porous Materials. *Adv. Mater.* **2011**, *23*, 599–623.
26. Jiang, X.; Ward, T. L.; Swol, F. Van; Brinker, C. J. Numerical Simulation of Ethanol-Water-Nacl Droplet Evaporation. *Ind. Eng. Chem. Res.* **2010**, *49*, 5631–5643.
27. Fontecave, T.; Boissiere, C.; Baccile, N.; Plou, F. J.; Sanchez, C. Using Evaporation-Induced Self-Assembly for the Direct Drug Templating of Therapeutic Vectors with High Loading Fractions, Tunable Drug Release, and Controlled Degradation. *Chem. Mater.* **2013**, *25*, 4671–4678.
28. Boissiere, C.; Grosso, D.; Amenitsch, H.; Gibaud, A.; Coupe, A.; Baccile, N.; Sanchez, C. First in-Situ SAXS Studies of the Mesostructuration of Spherical Silica and Titania Particles during Spray-Drying Process. *Chem. Commun.* **2003**, 2798.
29. Maa, Y.-F.; Prestrelski, S. J. Biopharmaceutical Powders Particle Formation and Formulation Considerations. *Curr. Pharm. Biotechnol.* **2000**, *1*, 283–302.
30. Braga, G. K.; Oliveira, W. P. Manufacturing Drug Loaded Chitosan Microspheres by Spray Drying: Development, Characterization, and Potential Use in Dentistry. *Dry. Technol.* **2007**, *25*, 303–310.
31. Freitas, C.; Müller, R. H. Spray-Drying of Solid Lipid Nanoparticles (SLN TM). *Eur. J. Pharm. Biopharm.* **1998**, *46*, 145–151.
32. Tsapis, N.; Bennett, D.; Jackson, B.; Weitz, D. A.; Edwards, D. A. Trojan Particles: Large Porous Carriers of Nanoparticles for Drug Delivery. *Proc. Natl. Acad. Sci. U.S.A.* **2002**, *99*, 12001–12005.
33. Langrish, T. A. G. New Engineered Particles from Spray Dryers: Research Needs in Spray Drying. *Drying Technol.* **2007**, *25*, 971–983.
34. Farid, M. A New Approach to Modelling of Single Droplet Drying. *Chem. Eng. Sci.* **2003**, *58*, 2985–2993.
35. Baca, H. K.; Carnes, E.; Singh, S.; Ashley, C.; Lopez, D.; Brinker, C. J. Cell-Directed Assembly of Bio/Nano Interfaces-a New Scheme for Cell Immobilization. *Acc. Chem. Res.* **2007**, *40*, 836–845.
36. Harper, J. C.; Khripin, C. Y.; Carnes, E. C.; Ashley, C. E.; Lopez, D. M.; Savage, T.; Jones, H. D. T.; Davis, R. W.; Nunez, D. E.; Brinker, L. M.; *et al*. Cell-Directed Integration into Three-Dimensional Lipid-Silica Nanostructured Matrices. *ACS Nano* **2010**, *4*, 5539–5550.
37. Vehring, R.; Foss, W. R.; Lechuga-Ballesteros, D. Particle Formation in Spray Drying. *J. Aerosol Sci.* **2007**, *38*, 728–746.
38. Huang, D. Modeling of Particle Formation during Spray Drying. *Eur. Dry. Conf. - EuroDrying'2011* **2011**, 26–28.
39. Okuyama, K.; Abdullah, M.; Lenggoro, I. W.; Iskandar, F. Preparation of Functional Nanostructured Particles by Spray Drying. *Adv. Powder Technol.* **2006**, *17*, 587–611.
40. Littringer, E. M.; Paus, R.; Mescher, A.; Schroettner, H.; Walzel, P.; Urbanetz, N. A. The Morphology of Spray Dried Mannitol Particles—the Vital Importance of Droplet Size. *Powder Technol.* **2013**, *239*, 162–174.
41. Bruinsma, P. J.; Kim, A. Y.; Liu, J.; Baskaran, S. Mesoporous Silica Synthesized by Solvent Evaporation: Spun Fibers and Spray-Dried Hollow Spheres. *Chem. Mater.* **1997**, *9*, 2507–2512.
42. Jiang, X.; Ward, T. L.; Cheng, Y.-S.; Liu, J.; Brinker, C. J. Aerosol Fabrication of Hollow Mesoporous Silica Nanoparticles and Encapsulation of L-Methionine as a Candidate Drug Cargo. *Chem. Commun.* **2010**, *46*, 3019–3021.
43. Mitchell, J.; Newman, S.; Chan, H.-K. In Vitro and in Vivo Aspects of Cascade Impactor Tests and Inhaler Performance: A Review. *AAPS PharmSciTech* **2007**, *8*, 237–248.
44. Mitchell, J. P.; Nagel, M. W. Cascade Impactors for the Size Characterization of Aerosols from Medical Inhalers: Their Uses and Limitations. *J. Aerosol Med.* **2003**, *16*, 341–377.
45. Israelachvili, J. N. *Intermolecular and Surface Forces*, 3rd ed.; Academic Press: San Diego, 2011; pp 1−704.
46. Dunphy, D. R.; Alam, T. M.; Tate, M. P.; Hillhouse, H. W.; Smarsly, B.; Collord, A. D.; Carnes, E.; Baca, H. K.; Kohn, R.; Sprung, M. Characterization of Lipid-Templated Silica and Hybrid Thin Film Mesophases by Grazing Incidence Small-Angle X-Ray Scattering. *Langmuir* **2009**, *25*, 9500–9509.
47. Reits, E. A.; Neefjes, J. J. From Fixed to FRAP: Measuring Protein Mobility and Activity in Living Cells. *Nat. Cell Biol.* **2001**, *3*, E145–E147.
48. Potma, E. O.; de Boeij, W. P.; Bosgraaf, L.; Roelofs, J.; van Haastert, P. J.; Wiersma, D. A. Reduced Protein Diffusion Rate by Cytoskeleton in Vegetative and Polarized Dictyostelium Cells. *Biophys. J.* **2001**, *81*, 2010–2019.
49. Mullineaux, C. W.; Nenninger, A.; Ray, N.; Robinson, C. Diffusion of Green Fluorescent Protein in Three Cell Environments in Escherichia coli. *J. Bacteriol.* **2006**, *188*, 3442–3448.
50. Oliver, W. C.; Pharr, G. M. Measurement of Hardness and Elastic Modulus by Instrumented Indentation: Advances in Understanding and Refinements to Methodology. *J. Mater. Res.* **2004**, *19*, 3–20.
51. Fan, H.; Hartshorn, C.; Buchheit, T.; Tallant, D.; Assink, R.; Simpson, R.; Kissel, D. J.; Lacks, D. J.; Torquato, S.; Brinker, C. J. Modulus-Density Scaling Behaviour and Framework Architecture of Nanoporous Self-Assembled Silicas. *Nat. Mater.* **2007**, *6*, 418–423.
52. Subhash, G.; Yao, S.; Bellinger, B.; Gretz, M. R. Investigation of Mechanical Properties of Diatom Frustules Using Nanoindentation. *J. Nanosci. Nanotechnol.* **2005**, *5*, 50–56.
53. Isaksson, H.; Nagao, S.; Małkiewicz, M.; Julkunen, P.; Nowak, R.; Jurvelin, J. S. Precision of Nanoindentation Protocols for Measurement of Viscoelasticity in Cortical and Trabecular Bone. *J. Biomech.* **2010**, *43*, 2410–2417.
54. Turner, C. H.; Rho, J.; Takano, Y.; Tsui, T. Y.; Pharr, G. M. The Elastic Properties of Trabecular and Cortical Bone Tissues Are Similar: Results from Two Microscopic Measurement Techniques. *J. Biomech.* **1999**, *32*, 437–441.
55. Sorelli, L.; Constantinides, G.; Ulm, F.-J.; Toutlemonde, F. The Nano-Mechanical Signature of Ultra High Performance Concrete by Statistical Nanoindentation Techniques. *Cem. Concr. Res.* **2008**, *38*, 1447–1456.
56. Bruet, B. J. F.; Qi, H. J.; Boyce, M. C.; Panas, R.; Tai, K.; Frick, L.; Ortiz, C. Nanoscale Morphology and Indentation of Individual Nacre Tablets from the Gastropod Mollusc Trochus niloticus. *J. Mater. Res.* **2011**, *20*, 2400–2419.
57. Amir, A.; Babaeipour, F.; McIntosh, D. B.; Nelson, D. R.; Jun, S. Bending Forces Plastically Deform Growing Bacterial Cell Walls. *Proc. Natl. Acad. Sci. U.S.A.* **2014**, *111*, 5778–5783.

58. Zhao, F.; Bi, X.; Hao, Y.; Liao, X. Induction of Viable but Nonculturable Escherichia coli O157:H7 by High Pressure CO_2 and Its Characteristics. *PLoS One* **2013**, *8*, e62388.
59. Berlin, D. L.; Herson, D. S.; Hicks, D. T.; Hoover, D. G. Response of Pathogenic Vibrio Species to High Hydrostatic Pressure. *Appl. Environ. Microbiol.* **1999**, *65*, 2776–2780.
60. Oliver, J. D. The Viable but Nonculturable State in Bacteria. *J. Microbiol.* **2005**, *43*, 93–100.
61. Jensen, S. E.; Hubrechts, P.; Klein, B. M.; Hasløv, K. R. Development and Validation of an ATP Method for Rapid Estimation of Viable Units in Lyophilised BCG Danish 1331 Vaccine. *Biologicals* **2008**, *36*, 308–314.
62. Lundin, A. Use of Firefly Luciferase in ATP-Related Assays of Biomass, Enzymes, and Metabolites. *Methods Enzymol.* **2000**, *305*, 346–370.
63. Hiraishi, Y.; Nandakumar, S.; Choi, S.-O.; Lee, J. W.; Kim, Y.-C.; Posey, J. E.; Sable, S. B.; Prausnitz, M. R. Bacillus Calmette-Guérin Vaccination Using a Microneedle Patch. *Vaccine* **2011**, *29*, 2626–2636.
64. U.S. Department of Health and Human Services/ Food and Drug Administration. *Guidance for Industry: Q1A(R2) Stability Testing of New Drug Substances and Products*; **2003**.
65. Oliver, J. D. Recent Findings on the Viable but Nonculturable State in Pathogenic Bacteria. *FEMS Microbiol. Rev.* **2010**, *34*, 415–425.
66. Heifets, L.; Linder, T.; Sanchez, T.; Spencer, D.; Brennan, J. Two Liquid Medium Systems, Mycobacteria Growth Indicator Tube and MB Redox Tube, for Mycobacterium tuberculosis Isolation from Sputum Specimens. *J. Clin. Microbiol.* **2000**, *38*, 1227–1230.